11-2019

Measurement of Electron Density and Temperature from Laser-induced Nitrogen Plasma at Elevated Pressure (1–6 bar)

Ashwin P. Rao

Mark Gragston

A Patnaik

Paul Hsu

Michael B. Shattan
Air Force Institute of Technology

Recommended Citation

Ashwin P. Rao, Mark Gragston, Anil K. Patnaik, Paul S. Hsu, and Michael B. Shattan, "Measurement of electron density and temperature from laser-induced nitrogen plasma at elevated pressure (1–6 bar)," Opt. Express 27, 33779-33788 (2019). https://doi.org/10.1364/OE.27.033779

Research Article | Vol. 27, No. 23 / 11 November 2019 / Optics Express 33779
Optics EXPRESS

Measurement of electron density and temperature from laser-induced nitrogen plasma at elevated pressure (1–6 bar)

ASHWIN P. RAO,[1] MARK GRAGSTON,[2] ANIL K. PATNAIK,[1] PAUL S. HSU,[3] AND MICHAEL B. SHATTAN[1,*]

[1]Department of Engineering Physics, Air Force Institute of Technology, Wright-Patterson AFB, OH 45433, USA
[2]Department of Mechanical, Aerospace, and Biomedical Engineering, University of Tennessee Space Institute, Tullahoma, TN 37388, USA
[3]Spectral Energies LLC, 4065 Executive Drive, Beavercreek, OH 45431, USA
[*]michael.shattan@afit.edu

Abstract: Laser-induced plasmas experience Stark broadening and shifts of spectral lines carrying spectral signatures of plasma properties. In this paper, we report time-resolved Stark broadening measurements of a nitrogen triplet emission line at 1–6 bar ambient pressure in a pure nitrogen cell. Electron densities are calculated using the Stark broadening for different pressure conditions, which are shown to linearly increase with pressure. Additionally, using a Boltzmann fit for the triplet, the electron temperature is calculated and shown to decrease with increasing pressure. The rate of plasma cooling is observed to increase with pressure. The reported Stark broadening based plasma diagnostics in nitrogen at high pressure conditions will be significantly useful for future studies on high-pressure combustion and detonation applications.

1. Introduction

Laser-induced breakdown spectroscopy (LIBS) is a widely used technique for the spectroscopic analysis of gaseous [1], liquid [2], and solid [3] targets that utilize laser-induced plasma as a spectroscopic source. LIBS has been especially useful for combustion diagnostics, providing information on the local equivalence ratio [1,4,5], as well as determining temperature of flames and heated gas flows [6–9]; this technique has also been used for simultaneously measuring and igniting combustible mixtures [5,10]. Interest in in-cylinder engines (up to 20 bar), gas turbine engines (up to 30 bar), detonations (up to a few hundred bars), thermal power stations (up to 42 bar), and planetary bodies (e.g., 90 bar at Venus) is driving spectroscopic investigations at high-pressure conditions. However, LIBS is very sensitive to conditions in which the plasma is generated, because effects such as spectral broadening or self-absorption are more prevalent at elevated pressure. Furthermore, recent work in this area has demonstrated that significant instability of the laser-induced plasma occurs at high-pressure conditions, impacting the measurement stability and precision [4]. To better understand how LIBS can be used for measurements under such high-pressure conditions, the plasma and spectral emission properties must be characterized to understand the physics of the laser-induced plasma [11]. Furthermore, short-gated LIBS is of particular interest for combustion analysis, where the measurement is taken approximately 100 ns after plasma creation but before more complex and highly-stochastic recombination processes dominate the signal [4,12].

For a typical LIBS measurement involving a gaseous sample, an intense pulsed laser is focused at the probe volume. The initial ionization at the target creates seed electrons that are accelerated by the remainder of pulse via inverse-Bremsstrahlung interactions [13,14], where the collisions between electrons accelerated by the laser field and, molecules and atoms significantly

#376874 https://doi.org/10.1364/OE.27.033779
Journal © 2019 Received 3 Sep 2019; revised 26 Sep 2019; accepted 29 Sep 2019; published 4 Nov 2019

Optics EXPRESS

increase, resulting in avalanche ionization [14,15]. The resulting plasma then expands and cools, with various recombination and chemical reaction pathways dynamically changing the plasma emission characteristics. Early in the plasma lifetime (approximately hundreds of nanoseconds), the emission is largely broadband, owing to free–free and free–bound electron transitions [14,15]. As the plasma expands and cools, discrete emission bands emerge. During this process, ionic emissions are prevalent early (≤100ns after the laser peak) but decay quickly, yielding emissions primarily of atomic neutrals followed by weak molecular lines as the gas returns to equilibrium [14,16].

These plasma emissions can be used to calculate many key plasma parameters essential for characterization. For example, the local electric field created by plasmas causes spectral broadening and line splitting. This phenomenon, known as the Stark effect, results in a broadening of the spectral line [17]. Thus, the Stark width of a spectral peak can be measured and used to calculate the electron density of the plasma. Additionally, the relative emission intensities of multiple spectral emissions from the same species can be analyzed to determine the corresponding excitation temperature. Under the partial local thermodynamic equilibrium conditions, this temperature will be equivalent to the electron temperature [18].

Nitrogen is abundant in combustion applications owing to its high concentration in the atmosphere. Hence, a large number of strong nitrogen spectral emission lines, such as the emission triplets at 566.6, 567.9, and 571.1 nm, are present in the LIBS signal of combustion mixtures; these emission lines are also free from spectral interference from other fuel elements, such as carbon and hydrogen. Thus, nitrogen is one of the ideal targets for diagnostic measurements in the laser-induced plasma. Although Stark effect on hydrogen Balmer lines has been extensively investigated in the literature, only a few studies have been reported on the Stark broadening of the $N_{II}(568)$ emission triplet to measure electron density and temperature [19,20]. Furthermore, to the best of our knowledge, the influence of elevated pressure on Stark broadening measurements has never been reported for determination of electron density. At elevated pressure, the Stark effect from the local electric field of plasmas is expected to become more pronounced, even for N_{II}. Enhanced Stark effect is caused by the increase in electron density with pressure. Only a few literature exists for plasma diagnostics at elevated pressures exceeding 1 bar [21]. In this work, we examine the Stark broadening of the N_{II} emission line (at around 568 nm) from a laser-induced nitrogen plasma at elevated pressure. Time-resolved spectra at various pressures are recorded, and electron densities are calculated from measured Stark width by using well-established relationships based on plasma parameters tabulated by Griem [22]. The deconvolved intensities of the N_{II} triplet emission lines at 566.6, 567.9, and 571.1 nm were determined; the Boltzmann distribution of the triplet is used to estimate the electron temperature under partial local thermodynamic equilibrium (pLTE) approximation. The Stark widths, electron densities, and electron temperatures are tabulated for pressures ranging from 1 to 6 bar.

The paper is organized as follows: in Sect. 2 the experimental setup for measurement of the N_{II} plasma emission at elevated pressure is presented; the spectral analysis methodology is described in Sect. 3; electron density and electron temperature measurements at elevated pressure are presented in Sects. 4 and 5, respectively; the results are summarized in Sect. 6.

2. Experiment setup

A schematic of the experimental setup used is shown in Fig. 1. An Nd:YAG laser (QuantaRay 290 Pro, Spectra-Physics) with an output wavelength of 532 nm and a pulse width of 10 ns provided pulses with an energy of 1200 mJ/pulse and a repetition frequency of 10 Hz. The laser energy was controlled with a half-wave plate and polarizing beam splitter setup to reduce the beam energy to 80 mJ/pulse in the experiment. The beam was focused at the center of the high-pressure cell by using a plano-convex lens with *f=+150 mm*. LIBS signals were collected using a second spherical lens with *f=+150 mm* to direct light to a 0.25 m spectrometer (SpectraPro

Optics EXPRESS

2300i, Princeton Instruments) equipped with a 1200 grooves/mm grating blazed at 500 nm. An ICCD camera (PI-MAX4, Princeton Instruments) with a 1024x1024 pixel array was used for the collection of LIBS emission spectra with a spectral dispersion of 12.8 μm per pixel.

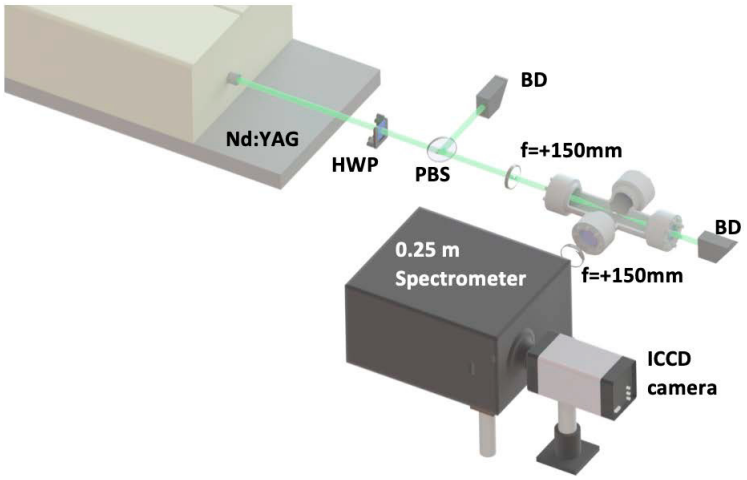

Fig. 1. Schematic diagram of setup for time-gated spectrally resolved plasma emission measurements. PBS: polarizing beam splitter; HWP: half wave plate; BD: beam dump

A tank of ultra-high purity nitrogen was coupled to the high-pressure cell. The pressure was regulated between 1–6 bars using a vacuum pump and manual gauges. The N_{II} spectra were recorded at camera gate delays from 60–260 ns (increasing by 40-ns steps) to monitor the temporal evolution of the electron density. All measurements were performed with a camera gate width of 20 ns for nitrogen. At each time delay, 150 frames of the spectra from the plasma were averaged for each pressure level.

3. Spectral analysis: extraction of the Stark width and determination of electron temperature

The Stark effect has been reported in the literature to produce both broadening of spectral lines as well as shifts of the central emission wavelength; both of these parameters can be used for plasma diagnostic measurements [16,17,19,20,22,23]. In the current experiment, although Stark broadening of the N_{II} emission line was pronounced across all pressures and gate-delay conditions in the recorded data, Stark shifts for this line were difficult to resolve and were often observable only at the earliest gate delay time, as reflected in Fig. 2. For example, the measured Stark shift of the N_{II} (568) line in Fig. 2 was approximately 0.03 nm, which was two orders of magnitude lower than the Stark broadening of this same line; similar behavior was reported by Konjevic *et. al.* under atmospheric pressure conditions [20]. In contrast, the Stark shifts in the hydrogen emission lines [23] are very prominent (on the order of nanometers). Consequently, the Stark shift of the 568-nm N_{II} line would be a poor diagnostic metric with very high level of uncertainty in electron density estimations. Hence, only the Stark broadening of N_{II} was chosen for diagnostics of electron density.

To conduct a baseline subtraction on the emission peak data, a signal removal method was employed. The background subtraction is critical to ensuring the accuracy of measurements calculated from the recorded spectral broadening and intensity parameters [24]. A Voigt profile fitting (VPF) routine was used to extract the Stark width for each peak, which was estimated as the Lorentzian width of the Voigt profile [25]. The deconvolution process accounted for all peaks

Optics EXPRESS

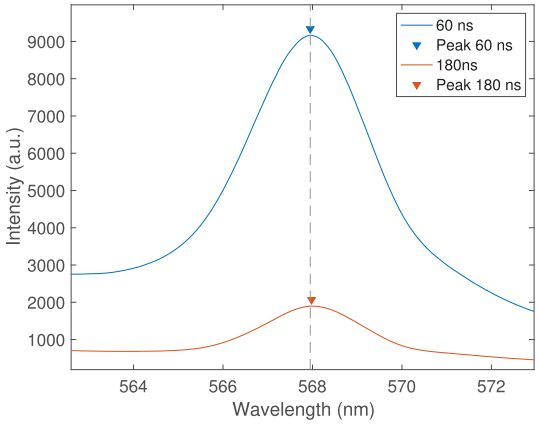

Fig. 2. Recorded raw spectral emission at 2 bar for camera delays 60 ns and 180 ns. The dashed grey line represents the peak position of the spectrum at 60 ns delay. The observed Stark shift (w.r.t. the grey line) is visibly negligible. In contrast, the observed Stark broadening changed distinctly at two delay conditions.

and their relative strengths of the nitrogen emission triplet centered around 568 nm, as shown in Fig. 3.

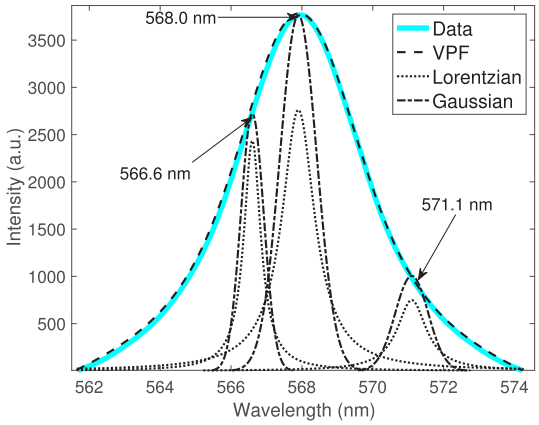

Fig. 3. Example of peak deconvolution at 60 ns gate delay and 4 bar ambient pressure. The calculated Gaussian and Lorentzian components are displayed for the 566.6, 567.9, and 571.1 nm lines, plotted along with the experimental spectra and the Voigt profile fit (VPF).

Electron densities were calculated using the Lorentzian width of the 568 nm emission line according to the following well-known empirical formula [15,26–28]:

$$n_e = \left(\frac{\lambda_{1/2}}{2w}\right) \times 10^{16}\text{cm}^{-3}. \tag{1}$$

In Eq. (1), $\lambda_{1/2}$ refers to the Stark full-width at half-maximum (FHWM), and w is the electron impact parameter, tabulated in Griem [22]. This method using the electron impact width parameter is commonly used to accurately calculate electron densities from the Stark width [15,26–28] and produces results that agree with other experimental measurements of Stark width for many different emission lines [20,22].

Optics EXPRESS

Furthermore, the Boltzman distribution of the deconvolved N_{II} triplet is used to extract electron temperature employing the following relation [29]:

$$\ln \frac{I^{ki}\lambda}{g_k A_{ki}} = \frac{-E_k}{k_B T} + \ln \frac{hcN}{U(T)} \tag{2}$$

The left-hand side of Eq. (2) can be plotted against different upper-level energy transitions (E_k) to generate a Boltzmann plot, where the slope is proportional to the inverse of the electron temperature [26]. The terms I^{ki}, λ, g_k, and A_{ki} refer to line intensity of the excited i^{th} degenerate k state, transition wavelength, excited energy level degeneracy, and transition probability for a given spectral emission line, respectively. These parameters were taken from the NIST Atomic Spectra Database [30]. The symbols E_k, k_B, T, h, c, N, and $U(T)$ refer to the upper level energy, Boltzmann constant, plasma temperature, Planck's constant, speed of light, total species population, and partition function, respectively. By plotting the left side of Eq. (2) against the energy corresponding to the excited state for the emission line, the temperature can be determined from the experimental data using a linear fit to calculate the slope. The reciprocal of the slope determines the electron temperature in eV [29].

It may be noted that the validity of the Boltzmann temperature method relies on the assumption of the plasma being in a partial local thermodynamic equilibrium (pLTE). To determine whether the laser-induced plasma was in pLTE, the McWhirter criterion [31]

$$n_e > 1.6 \times 10^{12} T^{1/2} \Delta E_{nm}^3 \tag{3}$$

is employed. Here, T is the plasma temperature (K) and E_{nm} is the transition energy (eV). Note that the Eq. (3) is a necessary but insufficient criterion for pLTE condition [18]. The existence of partial LTE is deduced from Eq. (3)–see Sect. 4 for details. The maximum and minimum electron densities estimated from Stark broadening are 2.8×10^{17} cm^{-3} and 1.5×10^{16} cm^{-3}, respectively. Using the maximum (2.6 eV) and minimum (0.4 eV) electron temperatures, the calculated values of the right-hand side of Eq. (3) ranges from 1.2 to 2.9×10^{15}. For the whole range, the left-hand side is at least one order of magnitude higher than the right-hand side; hence, the McWhirter criterion and hence pLTE condition is always met in our experiment [18,32].

4. Derivation of electron density from Stark broadening

The electron densities calculated using the extracted Stark widths using Eq. (1) at each pressure and gate delay are shown in Fig. 4. The error represents one standard deviation of the Stark width measured from 150 laser shots; this error was propagated through the electron density calculations using basic rules of uncertainty analysis. The fits for each data set had adjusted R^2 values of 0.9998, 0.9899, 0.9981, and 0.9972 for the atmospheric, 2, 4, and 6 bar conditions, respectively. The results clearly indicate that within 1–6 bar the electron density of the nitrogen plasma is linearly proportional to the Stark width of N_{II} (568) lines. This curve fitting, following the method used by Surmick and Parriger [23], was used to derive an empirical formula relating N_{II} Stark width and electron density, described in Eq. (4):

$$\Delta w = \beta(P) \left(\frac{n_e}{n_0}\right)^{1.01\pm0.05}. \tag{4}$$

Here, the first term $\beta(P)$ is an experimentally fitted function from Fig. 4 representing the effects of elevated pressure on Stark broadening, given by the equation

$$\beta(P) = 0.6206 e^{-0.034P}. \tag{5}$$

Here, P denotes the ambient pressure (bar), Δw is the Stark width (nm), n_e is the electron density (cm^{-3}), and n_0 is a normalization factor (10^{17} cm^{-3}). Equation (4) in conjunction with pressure

Optics EXPRESS

dependent exponential given in Eq. (5) represents a new empirical relation between the Stark width and electron density of a pure nitrogen plasma that includes the effects of ambient pressure from 1 to 6 bar. Equation (4) is accurate within a relative uncertainty of ±7% in measuring the electron density.

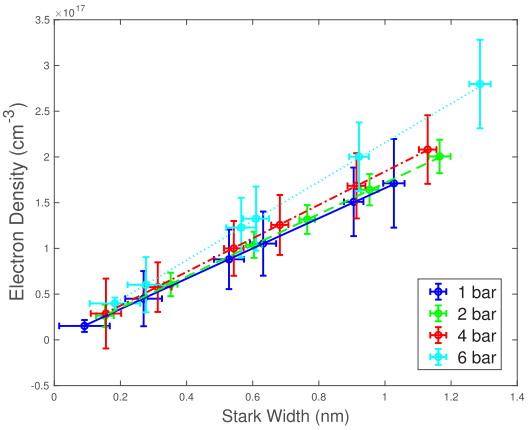

Fig. 4. Electron density as a function of Stark width across different pressures. A linear fit was applied for each data set to generate the Eq. (4).

Next, the temporal evolution of electron density in N_2 plasma is presented in Fig. 5 for 1–6 bar. Clearly, the increase in electron density with pressure is noticeable at earlier times and higher pressures (6 bar condition). The electron density is reduced at lower pressures and longer delays. Higher electron densities observed at earlier gate delays in the laser-induced plasma are dominated by avalanche ionization caused by inverse Brehmsstrahlung processes. These processes are typically accompanied by a significant increase in the Stark width of the spectral emission peaks as a result of the higher electron density [33,34]. As the plasma decays, the electron densities and the corresponding spectra resemble those of lower pressure cases, similar to the behavior seen in Fig. 5. These results indicate that the N_{II} line could be useful in air plasma diagnostic measurements from LIBS at higher pressures. However, the usefulness of this line could be limited at pressures exceeding 6 bar and earlier gate delays (<100 ns) because of higher

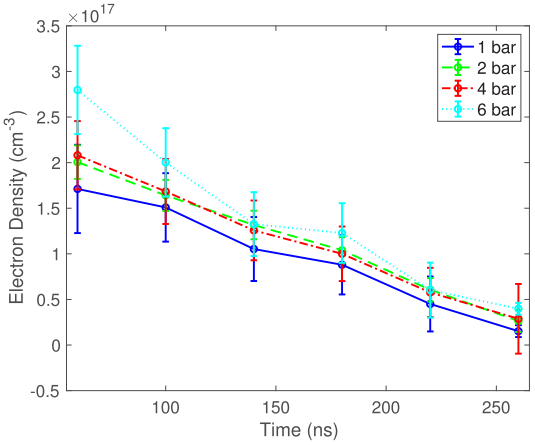

Fig. 5. Temporal evolution of electron density in a nitrogen plasma calculated at pressures from 1 to 6 bar.

Optics EXPRESS

signal instability. With increasing pressure, the intermolecular distance decreases, the collisional scattering cross section increases adding high level of stochasticity to the LIBS signal generation process. It should be noted that the electron density decays quicker at higher pressures, indicating that the plasma recombines and cools faster at higher ambient pressure levels, similar to that reported in Ref. [11].

5. Time-resolved measurement of electron temperature

The Boltzmann calculation method described in Sect. 3 was used to calculate the electron temperature from the time-resolved spectra obtained from the 150-shot-integrated peak intensity of the deconvolved 566.6, 567.9, and 571.1 nm emission lines starting at 60 ns gate delay and 40-ns intervals thereafter. The electron temperatures calculated from Eq. (2) are displayed in Fig. 6.

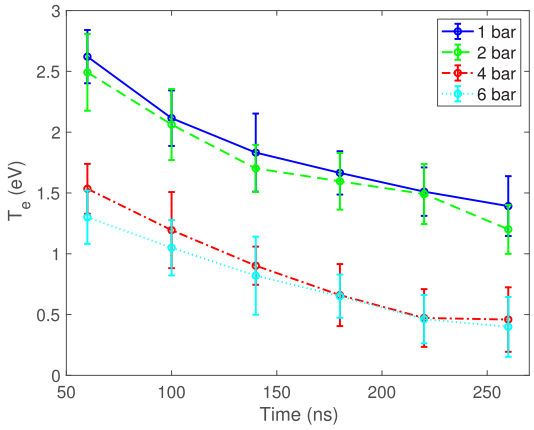

Fig. 6. Temporal evolution of electron temperature at different ambient pressures. Each temperature was determined from the slope of the Boltzmann plot generated using the line intensity data at the corresponding gate delay.

The results clearly indicate that the electron temperature is inversely proportional to the ambient gas pressure. The decay of plasma temperature T_e has been noted in several experimental studies [35–37]. At higher pressures, there is an increase in the collisional energy transfer between electrons and background gas, effectively reducing the temperature of the electrons. This pressure sensitivity is significant when the pressure is increased from 2 to 4 bar, but the trend is noticeably diminished at 6 bar. This diminished sensitivity could be because the electron densities generated at pressures above 4 bar are high enough to prevent an efficient recombination process, thus reducing the recombination rate that is important to lowering the overall plasma temperature. Using deconvolved emission line intensities, as opposed to resolved peak emission intensities, does affect the accuracy of the temperature measurements, as reflected in the larger statistical uncertainty of the temperature measurements mentioned previously. Additionally, the deviations increase as the pressure increases owing to this quenching process. The data in Fig. 6 also indicates that ambient pressure affects the overall electron temperature as well as the rate of plasma cooling. An exponential decay function was fit to each data set; the fit parameters are recorded in Table 1.

The tabulated fit results show that increasing ambient pressure causes T_e to decay faster. The exponential decay of the measured time-resolved electron temperature values from this experimental series agree with the data compiled by Zhang *et. al.* [35] for the early gate delay times observed in this work. The overall temperature change in this time period can range from

Optics EXPRESS

Table 1. Exponential fit parameters of equation $T_e = ae^{bt}$ for different ambient pressures.

Pressure (bar)	a	b
1	3.054	-0.0033
2	2.977	-0.0035
4	2.312	-0.0060
6	1.889	-0.0068

0.9–1.3 eV (10000–16000 K); as evident from the data in Fig. 6. All experimental data are summarized in Table 2 according to the gas pressure and gate delay. This table will help future high-pressure Stark effect investigations, where only limited literature exists that report any experimental investigation of nitrogen Stark broadening with respect to temperature and electron density.

Table 2. Summary of experimental data.

P (bar)	Gate Delay (ns)	T_e (eV)	n_e ($10^{17} cm^{-3}$)	Δw (nm)
1	60	2.621	1.712	1.027
	100	2.115	1.509	0.905
	140	1.832	1.053	0.632
	180	1.665	0.881	0.528
	220	1.511	0.450	0.270
	260	1.392	0.152	0.091
2	60	2.492	2.006	1.165
	100	2.062	1.641	0.953
	140	1.702	1.316	0.765
	180	1.596	1.039	0.604
	220	1.491	0.606	0.352
	260	1.201	0.263	0.153
4	60	1.534	2.081	1.129
	100	1.194	1.684	0.914
	140	0.902	1.257	0.682
	180	0.660	1.000	0.543
	220	0.472	0.577	0.313
	260	0.459	0.288	0.156
6	60	1.300	2.797	1.287
	100	1.049	2.002	0.922
	140	0.820	1.326	0.610
	180	0.651	1.228	0.565
	220	0.462	0.602	0.277
	260	0.399	0.398	0.183

6. Summary and conclusions

We have reported the measurement of time-resolved Stark broadening of laser-induced plasma at 1–6 bar in a high-pressure pure nitrogen cell. The Stark width of the $N_{II}(568)$ emission was employed to calculate the time-resolved electron density. We also derived an empirical formula

Optics EXPRESS

for the nitrogen N_{II} line to determine the electron density from the Stark width for the pressure range of 1–6 bar. Furthermore, we calculated the electron temperature from the Boltzmann plots of the experimental N_{II} triplet emission line intensities at elevated pressure. Our findings show that the electron temperature decreases with increasing ambient pressure, which could be due to the growing contributions of collisional energy transfer, whereas the rate of plasma cooling increased at higher pressures. Finally, the temperatures, densities, and Stark widths measured in this work were tabulated together, which may be helpful for future spectroscopic investigations of nitrogen in high-pressure reacting flows and plasmas [21].

One of the drawbacks of this investigation was the high uncertainty in Stark broadening, primarily due to the signal instability caused by avalanche ionization in the ns-laser induced plasma. Future experiments of laser-induced plasma employing picosecond or femtosecond pulsed lasers may be a solution to high-pressure signal instability [38], which could increase the accuracy of the Stark broadening at high-pressure conditions.

Funding

Air Force Office of Scientific Research (ENP19P906).

Acknowledgments

The authors sincerely thank Dr. Sukesh Roy for his thoughtful discussions on this project. Mr. Andy Kolonay of the Spectral Energies team was instrumental in assisting with experimental setup and hardware issues throughout the data collection campaign.

Disclosures

The authors declare no conflicts of interest.

References

1. Y. Wu, M. Gragston, Z. Zhang, P. S. Hsu, N. Jiang, A. K. Patnaik, S. Roy, and J. R. Gord, "High-pressure 1D fuel/air-ratio measurements with LIBS," Combust. Flame **198**, 120–129 (2018).
2. H. Suyanto, N. N. Rupiasih, W. T. B M. Manurung, and K. H. Kurniawan, "Qualitative analysis of Pb liquid sample using laser- induced breakdown spectroscopy (LIBS)," in *AIP Conference Proceedings*, vol. 1555, (2012), p. 14.
3. M. B. Shattan, M. Gragston, Z. Zhang, I. John D. Auxier, K. G. McIntosh, and C. G. Parigger, "Mapping of uranium in surrogate nuclear debris using laser-induced breakdown spectroscopy (LIBS)," Appl. Spectrosc. **73**(6), 591–600 (2019).
4. P. S. Hsu, M. Gragston, Y. Wu, Z. Zhang, A. K. Patnaik, J. Kiefer, S. Roy, and J. R. Gord, "Sensitivity, stability, and precision of quantitative Ns-LIBS-based fuel-air-ratio measurements for methane-air flames at 1–11 bar," Appl. Opt. **55**(28), 8042–8048 (2016).
5. T. X. Phuoc, "Laser-induced spark for simultaneous ignition and fuel-to-air ratio measurements," Opt. Lasers Eng. **44**(6), 520–534 (2006).
6. J. Lee, C. Bong, S. Lee, S. Im, and M. Bak, "Laser-induced breakdown thermometry via time-of-arrival measurements of associated acoustic waves," Appl. Phys. Lett. **113**(12), 123504 (2018).
7. T. W. Lee and N. Hegde, "Laser-induced breakdown spectroscopy for in situ diagnostics of combustion parameters including temperature," Combust. Flame **142**(3), 314–316 (2005).
8. J. Kiefer, J. Troeger, Z. Li, T. Seeger, M. Alden, and A. Leipertz, "Laser-induced breakdown flame thermometry," Combust. Flame **159**(12), 3576–3582 (2012).
9. A. P. Williamson, U. Thiele, and J. Kiefer, "Comparison of existing laser-induced breakdown thermometry techniques along with a time-resolved breakdown approach," Appl. Opt. **58**(14), 3950–3956 (2019).
10. H. Do, C. D. Carter, Q. Liu, T. M. Ombrello, S. Hammack, T. Lee, and K.-Y. Hsu, "Simultaneous gas density and fuel concentration measurements in a supersonic combustor using laser induced breakdown," Proc. Combust. Inst. **35**(2), 2155–2162 (2015).
11. A. K. Patnaik, Y. Wu, P. S. Hsu, M. Gragston, Z. Zhang, J. R. Gord, and S. Roy, "Simultaneous LIBS signal and plasma density measurement for quantitative insight into signal instability at elevated pressure," Opt. Express **26**(20), 25750–25760 (2018).
12. H. Do and C. Carter, "Hydrocarbon fuel concentration measurement in reacting flows using short-gated emission spectra of laser induced plasma," Combust. Flame **160**(3), 601–609 (2013).

Optics EXPRESS

13. Y. Wu, J. C. Sawyer, L. Su, and Z. Zhang, "Quantitative measurement of electron number in nanosecond and picosecond laser-induced air breakdown," J. Appl. Phys. **119**(17), 173303 (2016).
14. A. W. Miziolek, *Laser Induced Breakdown Spectroscopy* (Cambridge University, 2006).
15. D. Hahn and N. Omenetto, "Laser-Induced Breakdown Spectroscopy (LIBS), Part I: Review of Basic Diagnostics and Plasma-Particle Interactions: Still-Challenging Issues Within the Analytical Plasma Community," Appl. Spectrosc. **64**(12), 335A–336A (2010).
16. C. G. Parigger, A. C. Woods, and M. R. Rezaee, "Atomic hydrogen and molecular carbon emissions in laser-induced breakdown spectroscopy," J. Phys.: Conf. Ser. **397**, 012022 (2012).
17. H. Griem, *Spectral Line Broadening by Plasmas* (Academic Press, New York, 1974).
18. G. Cristoforetti, M. Aglio, and S. Legnaioli, "Local thermodynamic equilibrium in laser-induced breakdown spectroscopy: Beyond the McWhirter criterion," Spectrochim. Acta, Part B **65**(1), 86–95 (2010).
19. V. Milosavljevic and S. Djenize, "Measured Stark widths and shifts of NII, NIII and NIV spectral lines," Astron. Astrophys., Suppl. Ser. **128**(1), 197–201 (1998).
20. N. Konjevic and W. L. Wiese, "Experimental stark widths and shifts for spectral lines of neutral and ionized atoms," J. Phys. Chem. Ref. Data **19**(6), 1307–1385 (1990).
21. A. K. Patnaik, I. V. Adamovich, J. R. Gord, and S. Roy, "Recent advances in ultrafast-laser-based spectroscopy and imaging for reacting plasmas and flows," Plasma Sources Sci. Technol. **26**(10), 103001 (2017).
22. H. Griem, *Plasma Spectroscopy* (McGraw-Hill, New York, 1964).
23. D. M. Surmick and C. G. Parigger, "Empirical formulae for Electron Density Diagnostics from H_α and H_β Line Profiles," IRAMP **5**, 73–81 (2014).
24. G. Schulze, A. Jirasek, M. M. L. Yu, A. Lim, R. F. B. Turner, and M. W. Blades, "Investigation of selected baseline removal techniques as candidates for automated implementation," Appl. Spectrosc. **59**(5), 545–574 (2005).
25. M. Zaghloul, "Computing the Faddyeeva and Voigt functions," Software **38**, 103001 (2011).
26. M. Suchonova, P. Veis, J. Karhunen, P. Paris, M. Pribula, K. Piip, M. Laan, C. Porosnicu, C. Lungu, and A. Hakola, "Determination of deuterium depth profiles in fusion-relevant wall materials by nanosecond LIBS," Nucl. Mater. Energy **12**, 611–616 (2017).
27. M. A. Gondal, Y. W. Maganda, M. A. Dastageer, F. F. Al-Adel, and A. Naqvi, "Study of temporal evolution of electron density and temperature for atmospheric plasma generated from fluid samples using laser induced breakdown spectroscopy," in *2013 Saudi International Electronics, Communications and Photonics Conference*, (2013), pp. 1–4.
28. P. W. Tawfik, "Calibration free laser-induced breakdown spectroscopy (LIBS) identification of seawater salinity," Opt. Appl. **38**, 103001 (2007).
29. V. K. Unnikrishnan, K. Alti, V. Kartha, C. Santhosh, G. P. Gupta, and B. M. Suri, "Measurements of plasma temperature and electron density in laser-induced copper plasma by time-resolved spectroscopy of neutral atom and ion emissions," Pramana **74**(6), 983–993 (2010).
30. A. Kramida, Y. Ralchenko, and J. Reader, "NIST Atomic Spectra Database,".
31. R. McWhirter, *Plasma Diagnostic Techniques* (Academic Press, New York, 1965).
32. D. Boker and D. Bruggemann, "Temperature measurements in a decaying laser-induced plasma in air at elevated pressures," Spectrochim. Acta, Part B **66**(1), 28–38 (2011).
33. C. Goueguel, D. L. McIntyre, J. P. Singh, J. Jain, and A. K. Karamalidis, "Laser-induced breakdown spectroscopy (LIBS) of a high-pressure CO_2-water mixture: Application to carbon sequestration," Appl. Spectrosc. **68**(9), 997–1003 (2014).
34. A. Effenberger and J. R Scott, "Effect of atmospheric conditions on LIBS spectra," Sensors **10**(5), 4907–4925 (2010).
35. S. Zhang, X. Wang, M. He, Y. Jiang, B. Zhang, W. Hang, and B. Huang, "Laser-induced plasma temperature," Spectrochim. Acta, Part B **97**, 13–33 (2014).
36. M. A. Hafez, M. A. Khedr, F. F. Elaksher, and Y. E. Gamal, "Characteristics of Cu plasma produced by a laser interaction with a solid target," Plasma Sources Sci. Technol. **12**(2), 185–198 (2003).
37. S. S. Harilal, R. C. Issac, C. V. Bindhu, V. P. N. Nampoori, and C. P. G. Vallabhan, "Optical emission studies of species in laser-produced plasma from carbon," J. Phys. D: Appl. Phys. **30**(12), 1703–1709 (1997).
38. P. S. Hsu, A. K. Patnaik, A. J. Stoll, J. Estevadeordal, S. Roy, and J. R. Gord, "Femtosecond-laser-induced plasma spectroscopy for high-pressure gas sensing: enhanced stability of spectroscopic signal," Appl. Phys. Lett. **113**(21), 214103 (2018).